Robust Position Estimation using Range Measurements from Transmitters with Inaccurate Positions

Artun Sel
Electrical and Computer Engineering
The Ohio State University
Columbus, OH 43210, USA
sel.2@osu.edu

Samer Hayek
Electrical and Computer Engineering
The Ohio State University
Columbus, OH 43210, USA
watchihayek.1@osu.edu

Zaher M. Kassas
Electrical and Computer Engineering
The Ohio State University
Columbus, OH 43210, USA
zkassas@ieee.org

***Abstract*—The problem of position estimation using range measurements from transmitters with inaccurately known positions is considered. The true position of each transmitter is assumed to lie within a disk of a known radius, centered at the inaccurate position. A robust estimation framework is proposed, formulating a min-max optimization problem and presenting a tractable solution approach. A sensitivity map is constructed to quantify the positioning error in different regions due to inaccuracies in the transmitters' positions. Numerical simulations are presented demonstrating the construction and application of the sensitivity map for estimating the position of a mobile receiver. It is shown that the sensitivity map yields invaluable insights to the expected positioning error in various regions within the environment. Experimental results are presented of a vehicle navigating in a real-world GPS-jammed environment using pseudorange measurements from 7 cellular transmitters whose positions are inaccurately known. The vehicle's positioning error is justified utilizing the offline-generated sensitivity map.**

***Index Terms*—Robust estimation, positioning, navigation, signals of opportunity, radio SLAM**

I. Introduction

Autonomous navigation has witnessed major strides in the past few years. Many automotive manufacturers have incorporated some form of autonomous driving capabilities, or they have plans to do so. Alarmingly, there is a strong dependence on global navigation satellite systems (GNSS) in producing a position, velocity, and time (PVT) estimate of the vehicle in a global frame [1]. Access to GNSS signals may not be completely guaranteed, necessitating the development of alternative positioning and navigation approaches for back up or redundancy.

When GNSS signals are unusable or unreliable, other signals in the environment can be exploited for navigation [2]. Navigation with signals of opportunity (SOPs) has attracted significant attention recently [3]–[7]. In this context, the vehicle-mounted receiver makes range-type measurements (e.g., pseudorange, carrier phase, or Doppler) to the transmitters [8]–[11]. Navigation with SOPs has been demonstrated indoors [12], [13]; on ground vehicles [14], [15]; on unmanned aerial vehicles (UAVs) [16], [17]; high-altitude aircraft [18], [19]; and in GNSS-jammed environments [20], [21].

One of the challenges of exploiting SOPs is that the transmitters' position may not be known *a priori*. Radio simultaneous localization and mapping (radio SLAM) [22]–[24] offers a relief to this problem, whereby the receiver's states are simultaneously estimated with the transmitters' states [25]. Even when radio SLAM is employed, it is inevitable to experience periods during which the transmitters' positions are inaccurate. In addition, even when a map of the transmitters' positions is available, such maps always suffer from some level of error. As such, it is imperative to analyze the effect of inaccurate transmitters' positions on receiver positioning.

The recent literature has considered the effect of transmitter states' error and uncertainty on receiver positioning. In [26], the unknown clock skew was studied in the context of time-of-arrival (TOA) position estimation. In [27], measurement uncertainty and outlier detection were addressed. In [28], multipath component delay uncertainty was formulated as an optimization problem and a nearest neighbor-based method to estimate the receiver position was presented. In [29], clock synchronization and transmitter's location uncertainty in time-difference-of-arrival (TDOA) was studied by considering the transmitter's location errors as Gaussian distributed. In [30], trajectory estimation using phase measurements originating from fixed antennas located within the environment was discussed, where a grid-search was proposed to mitigate the effects of uncertainties. In [31], the transmitter position uncertainty using received signal strength (RSS)–angle-of-arrival (AOA) for static receiver position estimation was considered.

This paper considers the problem of receiver position estimation using range measurements from transmitters with inaccurate positions. The true position of each transmitter is assumed to lie within a disk of a known radius, centered at the inaccurate position. A robust estimation framework is proposed with a tractable solution, leading to evaluating

This work was supported in part by the National Science Foundation (NSF) under Grant 2240512, in part by the Air Force Office of Scientific Research (AFOSR) under Grant FA9550-22-1-0476, and in part by the U.S. Department of Transportation under Grant 69A3552348327 for the CARMEN+ University Transportation Center.

the sensitivities of various regions in the environment to the transmitter position inaccuracy, given transmitter uncertainty bounds. The robust estimation formulation, by its nature, is a nonconvex-nonconcave min-max-type optimization problem, to which no straightforward solution exists [32]. This paper develops a tractable method based on convex relaxation and smoothed gradient descent-ascent (GDA). This paper makes the following contributions. First, a method for solving the robust estimation problem is proposed, utilizing a smoothed-GDA-based approach. Second, for a given map of inaccurate transmitter positions and a known uncertainty bound within which the true position lies, a so-called sensitivity map is constructed. The map quantifies the positioning error in different regions due to inaccurate transmitters' positions. Numerical simulations are presented demonstrating the construction and application of the sensitivity map for estimating the position of a mobile receiver. It is shown that the sensitivity map yields invaluable insights to the expected positioning error in various regions within the environment. Experimental results are presented for a vehicle navigating in a real-world GPS-jammed environment using pseudorange measurements from 7 cellular transmitters whose positions are inaccurately known. The vehicle's positioning error is justified utilizing the offline-generated sensitivity map.

This paper is organized as follows. Section II describes the considered problem. Section III develops the proposed robust estimation framework and sensitivity map generation. Simulation and experimental results are given in Sections IV and V, respectively. Section VI gives concluding remarks.

II. Problem Description

For position estimation using range-type measurements, precise transmitter locations are crucial for accurate receiver positioning. While precise transmitter location may be readily available for dedicated beacons, such information may not be available for SOPs. As such, it is vital to understand the impact of transmitter location inaccuracy on receiver position estimation accuracy. For many SOPs of interest (e.g., cellular transmitters), an approximate transmitter position could be obtained, e.g., from online databases or from an offline mapping campaign [33]. As such, it is reasonable to assume some uncertainty bound on these positions. Given these bounds, this paper will identify regions to which receiver positioning is sensitive to inaccuracies in transmitter position.

Fig. 1 illustrates the problem considered in this paper. Imagine a vehicle navigating by making range-type measurements to three transmitters. Assume that the vehicle has an inaccurate knowledge of the transmitters' positions, denoted $\{\mathbf{r}'_{s_m}\}_{m=1}^3$, and assume the true transmitters' positions, denoted $\{\mathbf{r}_{s_m}\}_{m=1}^3$, to be within a disk of radius ε. Should the vehicle navigate in regions $\{R_i\}_{i=1}^3$, what is the expected positioning error? This paper analyzes the position estimation error sensitivity in different regions to inaccurate transmitter position. To this end, a systematic approach for constructing so-called "sensitivity map" of the environment is presented, which quantifies the positioning error in different regions.

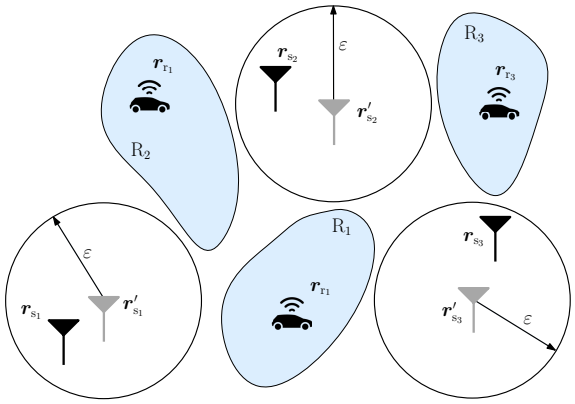

Fig. 1. A vehicle navigates with range-type measurements from three transmitters. The vehicle has an inaccurate knowledge of the transmitters' positions, denoted $\{\mathbf{r}'_{s_m}\}_{m=1}^3$. The true transmitters' positions, denoted $\{\mathbf{r}_{s_m}\}_{m=1}^3$, are known to lie within a disk of radius ε, centered at $\{\mathbf{r}'_{s_m}\}_{m=1}^3$. What is the expected positioning error in estimating the vehicle's position $\{\mathbf{r}_{r_i}\}_{i=1}^3$, should the vehicle navigate in regions $\{R_i\}_{i=1}^3$, respectively?

III. Robust Estimation Framework and Sensitivity Analysis of Inaccurate Transmitter Position

This section formulates the problem of positioning using range measurements from transmitters with inaccurately known positions via a robust estimation formalism, leading to generation of the sensitivity maps.

A. Convex Relaxation for the Nominal Estimation

Consider range-based position estimation of the receiver's position $\mathbf{r}_r \in \mathbb{R}^2$ in a two-dimensional (2-D) plane. The problem is considered in 2-D to simplify the analysis, with extension to 3-D readily achievable. The m$^{\text{th}}$ transmitter position is given by $\mathbf{r}_{s_m}$ and there are M such transmitters. The receiver makes range measurements $\{z_{s_m}\}_{m=1}^M$ to each transmitter, corrupted by additive Gaussian noise, i.e., $z_{s_m} = \|\mathbf{r}_{s_m} - \mathbf{r}_r\| + v_{s_m}$, with $v_{s_m} \sim \mathcal{N}(0, \sigma^2)$. For simplicity, assume the measurement noise to be independent and identically distributed.

When accurate transmitters' positions are available, the following "classic" optimization problem can be formulated

$$\min_{\hat{\mathbf{r}}_r} \sum_{m=1}^{M} (z_{s_m} - \|\mathbf{r}_{s_m} - \hat{\mathbf{r}}_r\|)^2, \tag{1}$$

where $\hat{\mathbf{r}}_r$ is the position estimate of the receiver. Problem (1) is in the form of least-squares, which is nonconvex. Consider the following convex relaxation. First, the cost function can be expanded and a new variable d_m is introduced, leading to the constrained optimization problem

$$\begin{aligned} \min_{\hat{\mathbf{r}}_r} \quad & \sum_{m=1}^{M} \left[(z_{s_m})^2 - 2z_{s_m} d_m + (d_m)^2\right] \\ \text{s.t.} \quad & d_m = \|\mathbf{r}_{s_m} - \hat{\mathbf{r}}_r\|, \quad m = 1, \ldots, M. \end{aligned} \tag{2}$$

By defining $\mathbf{d} = [d_1, \cdots, d_M]^\mathsf{T}$ and introducing the matrix $\mathbf{D} \in \mathbb{R}^{M\times M}$, the cost function can be expressed as an affine function, leading to

$$\begin{aligned} \min_{\hat{\mathbf{r}}_r} \quad & \sum_{m=1}^{M} \left[(z_{s_m})^2 - 2z_{s_m}d_m + D_{mm}\right] \\ \text{s.t.} \quad & D_{mm} - \left[\left(r_{s_{1_m}} - \hat{r}_{r_1}\right)^2 + \left(r_{s_{2_m}} - \hat{r}_{r_2}\right)^2\right] = 0, \\ & \mathbf{D} = \mathbf{d}\mathbf{d}^\mathsf{T}, \end{aligned} \tag{3}$$

where D_{mm} is the m^{th} diagonal element in $\mathbf{D}$.

By expanding the quadratic terms in the first constraint, and defining the matrix $\mathbf{Y} \in \mathbb{R}^{2\times 2}$, the first constraint can be expressed as an affine constraint, leading to

$$\begin{aligned} \min_{\hat{\mathbf{r}}_r} \quad & \sum_{m=1}^{M} \left[(z_{s_m})^2 - 2z_{s_m}d_m + D_{mm}\right] \\ \text{s.t.} \quad & D_{mm} - \sum_{k=1}^{2} \left(r^2_{s_{m_k}} - 2r_{s_{m_k}}\hat{r}_{r_k} + Y_{kk}\right) = 0, \\ & \mathbf{Y} = \hat{\mathbf{r}}_r\hat{\mathbf{r}}_r^\mathsf{T}, \\ & \mathbf{D} = \mathbf{d}\mathbf{d}^\mathsf{T}. \end{aligned} \tag{4}$$

Finally, the last two constraints can be relaxed by introducing the semi-definiteness constraints, leading to the following convex relaxation

$$\begin{aligned} \min_{\hat{\mathbf{r}}_r} \quad & \sum_{m=1}^{M} \left[(z_{s_m})^2 - 2z_{s_m}d_m + D_{mm}\right] \\ \text{s.t.} \quad & D_{mm} - \sum_{k=1}^{2} \left(r^2_{s_{m_k}} - 2r_{s_{m_k}}\hat{r}_{r_k} + Y_{kk}\right) = 0, \\ & \begin{bmatrix} \mathbf{D} & \mathbf{d} \\ \mathbf{d}^\mathsf{T} & 1 \end{bmatrix} \succeq 0, \quad \begin{bmatrix} \mathbf{Y} & \hat{\mathbf{r}}_r \\ \hat{\mathbf{r}}_r^\mathsf{T} & 1 \end{bmatrix} \succeq 0, \end{aligned} \tag{5}$$

where $\mathbf{D}$, $\mathbf{Y}$, and d_m are introduced to have an affine objective function in which $\|\mathbf{r}_{s_m} - \hat{\mathbf{r}}_r\|$ is substituted by d_m. Additionally, the matrix $\mathbf{D}$ is introduced to eliminate the d_m^2 term by first imposing the $d_m^2 = D_{mm}$ constraint and later relaxing it to the matrix inequality given by the third constraint. Problem (5) is convex, to which additional *a priori* information about the the receiver's position can be added as a convex constraint. The solution to (5) can be obtained via sequential quadratic programming (SQP). This formulation is necessary to initialize the nonconvex-nonconcave optimization problem to be introduced in the next section.

B. Robust Estimation as a min-max Problem

In this section, the receiver position estimation problem is formulated as an optimization problem, in which precise transmitter position $\mathbf{r}_{s_m}$ is unknown but the norm of the error between $\mathbf{r}_{s_m}$ and the "assumed" transmitter position $\mathbf{r}'_{s_m}$ is upper-bounded by ε in the form of $\|\mathbf{r}_{s_m} - \mathbf{r}'_{s_m}\| \leq \varepsilon$. The error vector is denoted by $\boldsymbol{\xi}_{s_m}$ and is given by

$$\mathbf{r}'_{s_m} = \mathbf{r}_{s_m} + \boldsymbol{\xi}_{s_m}. \tag{6}$$

Since the norm of the error is bounded by a known value, the following problem is introduced to incorporate this constraint, which is called robust estimation problem throughout this paper. The robust estimation problem can be stated as

$$\min_{\hat{\mathbf{r}}_r} \max_{\|\boldsymbol{\xi}_{s_m}\|\leq\varepsilon} \sum_{m=1}^{M} \left(z_m - \|\mathbf{r}'_{s_m} - \boldsymbol{\xi}_{s_m} - \hat{\mathbf{r}}_r\|\right)^2. \tag{7}$$

Problem (7) is a nonconvex-nonconcave min-max optimization problem [34]. The next subsection presents a convex relaxation method to facilitate the computation of $\hat{\mathbf{r}}_r$.

C. Convex Relaxation for the Outer Optimization Problem

The min-max optimization problem in (7) is in the form

$$\min_{x\in\mathcal{X}} \max_{y\in\mathcal{Y}} f(x, y), \tag{8}$$

where $x \in \mathcal{X}$ and $y \in \mathcal{Y}$ are the decision variables defined on their convex sets $\mathcal{X}$ and $\mathcal{Y}$, respectively. As for the objective function, $f(\bullet, y)$ is not convex with respect to x and $f(x, \bullet)$ is not concave with respect to y. This is more challenging than a nonconvex optimization problem in that even convergence to a local minima may not be achievable for a simple bilinear form [32], [35]. To facilitate computing a solution for the stated nonconvex-nonconcave min-max optimization problem in (7), the following approximation is introduced

$$\min_{x\in\mathcal{X}} \max_{i\in[1,N]} f(x, y_i), \tag{9}$$

where the $\{y_i\}_{i=1}^N$ terms are sampled from the feasible region associated with the variable. This problem can be relaxed as

$$\min_{x\in\mathcal{X}} \max_{\substack{\delta\in\Delta \\ \Delta=\left\{\delta|\delta_i\geq 0, \sum_i \delta_i = 1\right\}}} \sum_{i=1}^{N} \delta_i f(x, y_i), \tag{10}$$

where the introduced variable δ is defined on $\boldsymbol{\Delta}$, which is an N-dimensional probability simplex. This manipulation makes it possible to approximate the problem as a nonconvex-concave optimization, since the objective function is affine with respect to δ for a fixed x. The obtained form allows for the use of existing algorithms with convergence guarantees [36]–[38].

D. Smoothed GDA Algorithm

The nonconvex-concave min-max problem (8) can be solved with smooth gradient descent-ascent (GDA) algorithm where a proximal function is given by

$$K(x, z; y) = f(x, y) + \frac{p}{2}\|x - z\|_2^2, \tag{11}$$

where the proximal quadratic term (second term on the right-hand side of (11)) contains the variable z, which can be considered as the delayed version of x. The quadratic term is added to the original objective function to eliminate the oscillation behavior during the iteration, and p is a positive constant. The smoothed GDA algorithm is given in Algorithm 1, where the operators $\mathbf{P}_\mathcal{X}$ and $\mathbf{P}_\mathcal{Y}$ represent the projection operations and since the defined sets $\mathcal{X}$ and $\mathcal{Y}$ are convex, these operations can be expressed as a convex optimization problem [39].

The proposed method to solve the robust estimation problem in (7) is described in Algorithm 2, whereby the original problem is first approximated by a nonconvex-concave min-max optimization, which is solved by applying the smoothed-GDA Algorithm after constructing the proximal function stated in the second step of Algorithm 2.

Algorithm 1 Smoothed GDA

Initialization: Given x^0, z^0, y^0 and $0 < \beta \leq 1$.
for $t = 0, 1, 2, \ldots$ **do**
  $x^{t+1} \leftarrow \mathbf{P}_{\mathcal{X}}(x^t - c\nabla_x K(x^t, z^t; y^t))$
  $y^{t+1} \leftarrow \mathbf{P}_{\mathcal{Y}}(y^t + \alpha\nabla_y K(x^{t+1}, z^t; y^t))$
  $z^{t+1} \leftarrow z^t + \beta(x^{t+1} - z^t)$
end for

Algorithm 2 Robust Estimation Algorithm to Solve (7)

Initialization: Given $\{\mathbf{r}'_{s_m}\}_{m=1}^M$ and ε
Sample N_s $\{\xi_{s_m}\}_{m=1}^M$ s.t. they are bounded by ε
Assign $\sum_{j=1}^{N_s} \delta^{(j)} \sum_{m=1}^M \left(z_{s_m} - \left\|\left[\mathbf{r}'_{s_m} - \xi_{s_m}^{(j)}\right] - \hat{\mathbf{r}}_r\right\|\right)^2$ to $K(\hat{\mathbf{r}}_r, \hat{\mathbf{r}}'_r; \delta)$
Initialize $\hat{\mathbf{r}}_r^0$ by solving (5).
Initialize $\hat{\mathbf{r}}_r'^0 \leftarrow \hat{\mathbf{r}}_r^0$ and, $\delta^0 \in \mathbf{\Delta}$
Initialize $0 < \beta \leq 1$, $\alpha > 0$, $c > 0$
for $t = 0, 1, 2, \ldots$ **do**
  $\hat{\mathbf{r}}_r^{t+1} \leftarrow P_Y(\hat{\mathbf{r}}_r^t - c\nabla_{\hat{\mathbf{r}}_r} K(\hat{\mathbf{r}}_r^t, \hat{\mathbf{r}}_r'^t; \delta^t))$
  $\delta^{t+1} \leftarrow P_\Delta(\delta^t + \alpha\nabla_\delta K(\hat{\mathbf{r}}_r^{t+1}, \hat{\mathbf{r}}_r'^t; \delta^t))$
  $\hat{\mathbf{r}}_r'^{t+1} \leftarrow \hat{\mathbf{r}}_r'^t + \beta(\hat{\mathbf{r}}_r^{t+1} - \hat{\mathbf{r}}_r'^t)$
end for

E. Sensitivity Map Computation

The proposed algorithm to construct the sensitivity map for receiver positioning with inaccurately known transmitters' positions is given in Algorithm 3.

Algorithm 3 Sensitivity Map Construction

Initialization: Given $\{\mathbf{r}'_{s_m}\}_{m=1}^M$ and ε
Initialize $0 < \beta \leq 1$, $\alpha > 0$, $c > 0$.
for each point $\mathbf{r}_r$ in the environment **do**
  sample N_1 $\{\mathbf{r}_{s_m}\}_{m=1}^M$ s.t. they are bounded by ε
  for each $\{\mathbf{r}_{s_m}\}_{m=1}^M$ set **do**
    compute $\hat{\mathbf{r}}_r$ by Algorithm 2
  end for
  find a simplex that contains N such $\hat{\mathbf{r}}_r$ points
  find the center of the simplex and assign it to $\hat{\mathbf{r}}_r$
  find the error $\|\mathbf{r}_r - \hat{\mathbf{r}}_r\|$
end for

IV. Numerical Simulations

This section presents numerical simulation results demonstrating the construction of the sensitivity map and robust estimation formulation proposed in Section III. The numerical simulations are inspired by the results achieved in [20], [21], in which a ground vehicle navigated with pseudorange measurements to SOP transmitters in a GPS-jammed environment. In contrast to the formulation presented in [20], [21], in which the SOP transmitter positions were known to the navigating vehicle, this section relaxes this assumption and considers inaccurate transmitter positions. To this end, the sensitivity map is computed as described in Algorithm 3 to assess the sensitivity levels of different regions in the environment to transmitter position inaccuracies. Next, the positioning performance for a set of trajectories are compared. First, for a given set of inaccurate transmitter locations, the sensitivity maps are created for a certain uncertainty bound. Fig. 2 shows the sensitivity map for $\varepsilon = 245$ m, which corresponds to the 95% uncertainty covariance of $\mathbf{P} = (10^4)\mathbf{I}_{2\times 2}$ around the inaccurate transmitter's position [40]. The inaccurate transmitters' positions were chosen randomly within a disk of radius ε from the true transmitters' positions. The sensitivity map essentially quantifies the positioning error at each candidate receiver position in the environment, making range measurements to each inaccurate transmitter position.

Next, three receiver trajectories with different initial positions within the environment but the same initial velocities $\dot{\mathbf{r}}_r(0) = [28.06, -2.34]^\mathsf{T}$ were generated. The receiver's dynamics was assumed to evolve according to a nearly constant velocity with acceleration process noise power spectral densities $\tilde{q}_x = \tilde{q}_y = 0.01$ m^2/s^3 [20]. For each trajectory, range measurements at a sampling period of $T = 0.01$ s were generated to the transmitter's true position, corrupted by additive zero-mean Gaussian noise with variance $\sigma^2 = 10^{-3}$ m^2. An extended Kalman filter (EKF) was used to fuse the range measurements to estimate the receiver's states $\mathbf{x} = \left[\mathbf{r}_r^\mathsf{T}, \dot{\mathbf{r}}_r^\mathsf{T}\right]^\mathsf{T}$. The EKF used the inaccurate transmitters' positions and was initialized as $\hat{\mathbf{x}}(0|0) \sim \mathcal{N}[\mathbf{x}(0), \mathbf{P}(0|0)]$, where $\mathbf{P}(0|0) = \text{diag}[10, 10, 1, 1]$. Fig. 2 shows the three simulated trajectories and Table I gives the receiver's position root mean squared errors (RMSEs). Among the three trajectories, the position RMSE of Trajectory 3 was the lowest, since it is located in a less sensitive region, while Trajectory 2 suffered from the highest position RMSE.

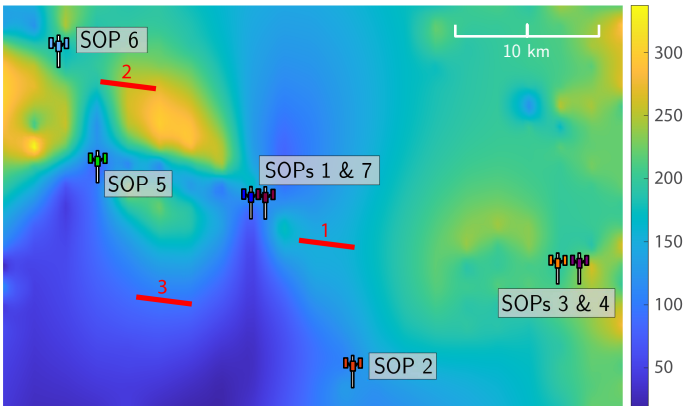

Fig. 2. The sensitivity map for inaccurate SOP transmitter positions and the three simulated trajectories (in red).

TABLE I
Position RMSE of the Three Receiver Trajectories in Fig. 2

Trajectory	Position RMSE [m]
Trajectory 1	131.91
Trajectory 2	182.26
Trajectory 3	104.84

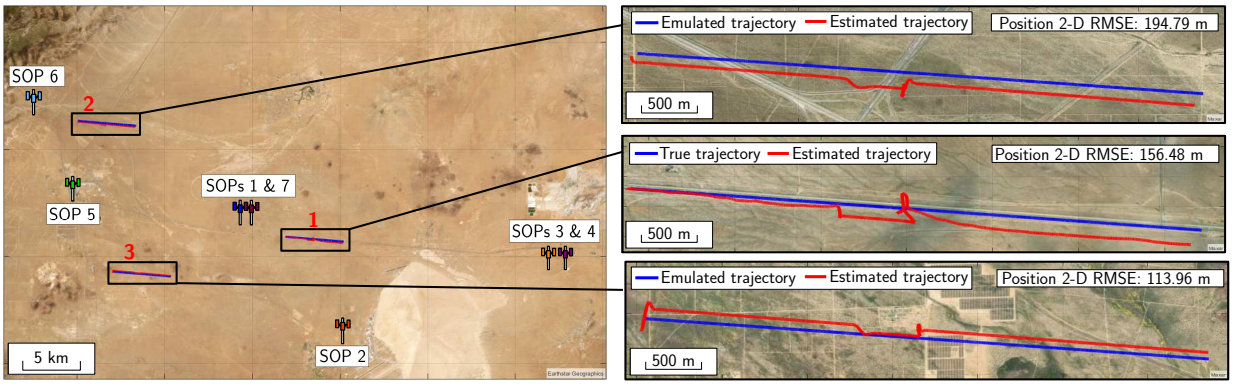

Fig. 3. True, estimated, and emulated trajectories.

V. Experimental Results

This section presents experimental results in a real-world GPS-jammed environment. To this end, a ground vehicle, was equipped with a National Instrument (NI) universal software radio peripheral (USRP), two consumer-grade Laird cellular antennas, laptop, and a Septentrio GNSS-INS, comprising a multifrequency GNSS AsteRx-i V receiver, an industrial-grade Vectornav VN-100 micro-electromechanical system (MEMS) inertial measurement unit (IMU), and a dual-GNSS antenna system. The vehicle-mounted GNSS-IMU was used to obtain the vehicle's ground truth trajectory, utilizing signals from non-jammed GNSS constellations (Galileo and GLONASS). The USRP utilized a GNSS-disciplined oscillator (GNSSDO) and was tuned to listen to two carrier frequencies corresponding to the U.S. cellular providers: Verizon Wireless and T-Mobile. The receiver discussed in [21] was used to obtain pseudorange measurements to 7 cellular SOPs. Since the measurements were in the form of pseudoranges, the following approach was adopted to convert them to ranges, which would enable comparison against the simulation results presented in Section IV. Given the vehicle's ground truth trajectory and the true transmitters' positions, a forward-pass Kalman filter was used to estimate the history of the clock error between the receiver and each SOP transmitter along the vehicle's trajectory. These estimates were then subtracted from the measured pseudoranges, to yield "range" measurements.

In contrast to the results in [21], which considered known transmitters' positions and a different part of the vehicle's trajectory, the results herein relax this assumption and show results with inaccurate transmitter positions. The inaccurate 2-D transmitters' positions were randomly sampled from within a disk of radius $\varepsilon = 245$ m, centered at the true transmitters' positions, while the inaccuracy in the vertical direction was made very small, due to poor vertical dilution of precision considerations. Table II gives the position errors between the SOP transmitters' positions and the inaccurate ones.

Next, the range measurements were fused via the EKF described in [20]. Since the vehicle was driven along Trajectory 1 shown in Fig. 3, and in order to analyze the error along other trajectories in the environment, two trajectories (denoted by 2 and 3 in Fig. 3) were emulated as follows. Range measurements were generated to the same inaccurate SOP transmitter positions, corrupted by the same noise time history from Trajectory 1 (obtained by subtracting the true range and estimated clock errors from the pseudorange measurements). It can be seen from Fig. 3 that the trajectory's relative position RMSEs are consistent with what was achieved in the simulation results, namely Trajectory 3 yielded the least position RMSE, while Trajectory 2 yielded the highest position RMSE, which can be justified by the sensitivity map.

TABLE II
SOP Transmitter Position Errors

Transmitter ID	Position Error [m]	Transmitter ID	Position Error [m]
SOP 1	226.88	SOP 2	197.23
SOP 3	48.37	SOP 4	141.15
SOP 5	95.87	SOP 6	120.23
SOP 7	53.25		

VI. Conclusion

This paper analyzed the problem of receiver positioning with terrestrial transmitters whose positions are inaccurately known. To this end, the problem was formulated as a robust optimization problem, to which a tractable solution was proposed, leading to generation of sensitivity maps. Numerical results were presented demonstrating the application of the formulation. Experimental results in a real-world GPS-jammed environment were presented, rationalizing the achieved navigation accuracy via the proposed sensitivity map.

VII. Acknowledgments

The authors thank C. Lee at Edwards Air Force Base for inviting the ASPIN Laboratory to conduct experiments during NAVFEST. The authors also thank J. Khalife, A. Abdallah, J. Morales, K. Shamaei, M. Maaref, K. Semelka, M. Nguyen, and T. Mortlock for their help with data collection.

References

[1] Z. Kassas, P. Closas, and J. Gross, "Navigation systems for autonomous and semi-autonomous vehicles: Current trends and future challenges," *IEEE Aerospace and Electronic Systems Magazine*, vol. 34, no. 5, pp. 82–84, May 2019.

[2] N. Souli, P. Kolios, and G. Ellinas, "Online relative positioning of autonomous vehicles using signals of opportunity," *IEEE Transactions on Intelligent Vehicles*, vol. 7, no. 4, pp. 873–885, 2022.

[3] M. Maaref and Z. Kassas, "Ground vehicle navigation in GNSS-challenged environments using signals of opportunity and a closed-loop map-matching approach," *IEEE Transactions on Intelligent Transportation Systems*, vol. 21, no. 7, pp. 2723–2723, July 2020.

[4] R. Whiton, "Cellular localization for autonomous driving: A function pull approach to safety-critical wireless localization," *IEEE Vehicular Technology Magazine*, vol. 17, no. 4, pp. 28–37, 2022.

[5] A. Brevick, K. Strandjord, and P. Wang, "Evaluating navigation augmentation with LTE in the urban signal environment," in *Proceedings of ION International Technical Meeting*, January 2023, pp. 1154–1168.

[6] M. Hameed, M. Philips-Blum, M. Arizabaleta-Diez, and T. Pany, "LTE transmitter states estimation using a combined code and carrier phase observation model," in *Proceedings of IEEE/ION Position, Location, and Navigation Symposium*, April 2023, pp. 1107–1117.

[7] T. Jin, F. Li, H. Qin, and D. Liu, "Differential time of arrival based opportunistic positioning for asynchronous cellular signals: Model, algorithms and experiments," *IEEE Transactions on Vehicular Technology*, vol. 72, no. 10, pp. 12 983–12 999, October 2023.

[8] K. Shamaei and Z. Kassas, "Receiver design and time of arrival estimation for opportunistic localization with 5G signals," *IEEE Transactions on Wireless Communications*, vol. 20, no. 7, pp. 4716–4731, 2021.

[9] P. Wang, Y. Wang, and J. Morton, "Signal tracking algorithm with adaptive multipath mitigation and experimental results for LTE positioning receivers in urban environments," *IEEE Transactions on Aerospace and Electronic Systems*, vol. 58, no. 4, pp. 2779–2795, August 2022.

[10] J. Tian, L. Fangchi, T. Yafei, and L. Dongmei, "Utilization of non-coherent accumulation for LTE TOA estimation in weak LOS signal environments," *EURASIP Journal on Wireless Communications and Networking*, vol. 2023, no. 1, pp. 1–31, 2023.

[11] R. Whiton, J. Chen, and F. Tufvesson, "Wiometrics: Comparative performance of artificial neural networks for wireless navigation," *IEEE Transactions on Vehicular Technology*, pp. 1–16, 2024, accepted.

[12] A. Abdallah, C. Jao, Z. Kassas, and A. Shkel, "A pedestrian indoor navigation system using deep-learning-aided cellular signals and ZUPT-aided foot-mounted IMUs," *IEEE Sensors Journal*, vol. 22, no. 6, pp. 5188–5198, March 2022.

[13] M. Pan, P. Liu, S. Liu, W. Qi, Y. Huang, X. You, X. Jia, and X. Li, "Efficient joint DOA and TOA estimation for indoor positioning with 5G picocell base stations," *IEEE Transactions on Instrumentation and Measurement*, vol. 71, pp. 1–19, 2022.

[14] R. Whiton, J. Chen, T. Johansson, and F. Tufvesson, "Urban navigation with LTE using a large antenna array and machine learning," in *Proceedings of IEEE Vehicular Technology Conference*, 2022, pp. 1–5.

[15] C. Yang, M. Arizabaleta-Diez, P. Weitkemper, and T. Pany, "An experimental analysis of cyclic and reference signals of 4G LTE for TOA estimation and positioning in mobile fading environments," *IEEE Aerospace and Electronic Systems Magazine*, vol. 37, no. 9, pp. 16–41, 2022.

[16] A. Abdallah and Z. Kassas, "UAV navigation with 5G carrier phase measurements," in *Proceedings of ION GNSS Conference*, September 2021, pp. 3294–3306.

[17] J. del Peral-Rosado, P. Nolle, F. Rothmaier, S. Razavi, G. Lindmark, X. Jiang, D. Shrestha, F. Gunnarsson, S. Parsawar, R. Mundlamuri, F. Kaltenberger, N. Sirola, O. Sarkka, U. Noman, J. Rostrom, K. Vaarala, P. Miettinen, S. Garlaschi, L. Canzian, H. Babaroglu, E. Rastorgueva-Foi, M. Turunen, J. Talvitie, and D. Flachs, "Proof-of-concept of dedicated aerial 5G and GNSS testbed for enhanced hybrid positioning," in *Proceedings of ION GNSS Conference*, September 2022, pp. 2362–2376.

[18] Z. Kassas, J. Khalife, A. Abdallah, C. Lee, J. Jurado, S. Wachtel, J. Duede, Z. Hoeffner, T. Hulsey, R. Quirarte, and R. Tay, "Assessment of cellular signals of opportunity for high-altitude aircraft navigation," *IEEE Aerospace and Electronic Systems Magazine*, vol. 37, no. 10, pp. 4–19, October 2022.

[19] Z. Kassas, J. Khalife, A. Abdallah, C. Lee, J. Jurado, J. Duede, Z. Hoeffner, T. Hulsey, R. Quirarte, S. Wachtel, and R. Tay, "Flight demonstration of high altitude aircraft navigation with cellular signals," *IEEE Intelligent Transportation Systems Magazine*, vol. 15, no. 4, pp. 150–165, 2023.

[20] Z. Kassas, J. Khalife, A. Abdallah, and C. Lee, "I am not afraid of the GPS jammer: resilient navigation via signals of opportunity in GPS-denied environments," *IEEE Aerospace and Electronic Systems Magazine*, vol. 37, no. 7, pp. 4–19, July 2022.

[21] Z. Kassas and A. Abdallah, "No GPS no problem: Exploiting cellular OFDM-based signals for accurate navigation," *IEEE Transactions on Aerospace and Electronic Systems*, vol. 59, no. 6, pp. 9792–9798, December 2023.

[22] C. Yang and A. Soloviev, "Simultaneous localization and mapping of emitting radio sources-SLAMERS," in *Proceedings of ION GNSS Conference*, September 2015, pp. 2343–2354.

[23] J. Morales, J. Khalife, and Z. Kassas, "Information fusion strategies for collaborative inertial radio SLAM," *IEEE Transactions on Intelligent Transportation Systems*, vol. 23, no. 8, pp. 12 935–12 952, August 2022.

[24] D. Beatty and M. Psiaki, "Analysis of long-range LTE radio-SLAM navigation approximated as a periodic system," in *Proceedings of ION GNSS Conference*, September 2022, pp. 1046–1061.

[25] Z. Kassas and T. Humphreys, "Observability analysis of collaborative opportunistic navigation with pseudorange measurements," *IEEE Transactions on Intelligent Transportation Systems*, vol. 15, no. 1, pp. 260–273, February 2014.

[26] Y. Zou, Q. Wan, and H. Liu, "TOA source node self-positioning with unknown clock skew in wireless sensor networks," in *Proceedings of IEEE International Conference on Acoustics, Speech and Signal Processing*, May 2019, pp. 4385–4389.

[27] P. Lutz, M. Schuster, and F. Steidle, "Visual-inertial SLAM aided estimation of anchor poses and sensor error model parameters of UWB radio modules," in *Proceedings of International Conference on Advanced Robotics*, December 2019, pp. 739–746.

[28] J. Chen, M. Zhu, and F. Tufvesson, "SLAM using LTE multipath component delays," in *Proceedings of IEEE Vehicular Technology Conference*, May 2020, pp. 1–5.

[29] Y. Zou and H. Liu, "Semidefinite programming methods for alleviating clock synchronization bias and sensor position errors in TDOA localization," *IEEE Signal Processing Letters*, vol. 27, pp. 739–746, 2020.

[30] A. Chatzistefanou, A. Tzitzis, S. Megalou, G. Sergiadis, and A. Dimitriou, "Trajectory-tracking of UHF RFID tags, exploiting phase measurements collected from fixed antennas," *IEEE Journal of Radio Frequency Identification*, vol. 5, no. 2, pp. 191–206, 2021.

[31] Q. Wang, X. Jiang, and F. Li, "Wireless localization using combined RSS-AOA measurements with anchor position uncertainty," in *Proceedings of International Conference on Frontiers Technology of Information and Computer*, December 2022, pp. 659–662.

[32] A. Han, B. Mishra, P. Jawanpuria, and J. Gao, "Nonconvex-nonconcave min-max optimization on Riemannian manifolds," *Transactions on Machine Learning Research*, pp. 1–33, 2023.

[33] J. Morales and Z. Kassas, "Optimal collaborative mapping of terrestrial transmitters: receiver placement and performance characterization," *IEEE Transactions on Aerospace and Electronic Systems*, vol. 54, no. 2, pp. 992–1007, April 2018.

[34] M. Razaviyayn, T. Huang, S. Lu, M. Nouiehed, M. Sanjabi, and M. Hong, "Nonconvex min-max optimization: Applications, challenges, and recent theoretical advances," *IEEE Signal Processing Magazine*, vol. 37, no. 5, pp. 55–66, 2020.

[35] V. Khattar, Y. Ding, B. Sel, J. Lavaei, and M. Jin, "A CMDP-within-online framework for meta-safe reinforcement learning," in *Proceedings of International Conference on Learning Representations*, January 2023, pp. 1–49.

[36] J. Zhang, P. Xiao, R. Sun, and Z. Luo, "A single-loop smoothed gradient descent-ascent algorithm for nonconvex-concave min-max problems," in *Proceedings of the Annual Conference on Advances in Neural Information Processing Systems*, 2020, pp. 1–13.

[37] J. Yang, A. Orvieto, A. Lucchi, and N. He, "Faster single-loop algorithms for minimax optimization without strong concavity," in *Proceedings of International Conference on Artificial Intelligence and Statistics*, 2022, pp. 1–33.

[38] S. Gu, B. Sel, Y. Ding, L. Wang, Q. Lin, M. Jin, and A. Knoll, "Balance reward and safety optimization for safe reinforcement learning: A perspective of gradient manipulation," in *Proceedings of AAAI Conference on Artificial Intelligence*, 2024, pp. 21 099–21 106.

[39] G. Yang, Y. Yan, H. Wang, and X. Shen, "Improved robust TOA-based source localization with individual constraint of sensor location uncertainty," *Signal Processing*, vol. 196, pp. 1–13, 2022.

[40] W. Hoover and M. Rockville, "Algorithms for confidence circles and ellipses," U.S. Department of Commerce, National Oceanic Atmospheric Administration, Washington, DC, USA, National Ocean Service (NOS) 107 Coast & Geodetic Survey (CGS) 3, 1984.